Three-body approach to $NN \rightarrow N\Delta$ reaction

T. Mizutani
Department of Physics, Virginia Polytechnic Institute and State University, Blacksburg, Virginia 24061

C. Fayard and G. H. Lamot
Institut de Physique Nucléaire de Lyon, Institut National de Physique Nucléaire et de Physique des Particules, Centre National de la Recherche Scientifique, Université Claude Bernard, F-69622 Villeurbanne CEDEX, France

B. Saghai
Service de Physique Nucléaire, Centre d'Etudes Nucléaires de Saclay, F-91191 Gif-sur-Yvette CEDEX, France
(Received 15 July 1992)

The $NN \rightarrow N\Delta$ reaction is investigated within the coupled πNN-NN theory. The model predictions for the differential cross section, production asymmetry, and spin-correlation parameters are compared with the Argonne data at $T_N^{\rm lab} = 0.57$, 0.81, and 1.01 GeV. Short-range effects are introduced through the ρ-exchange contribution. The overall quality of the results is satisfactory, except for the triplet part of the production asymmetry at the two highest energies. The role of the $^3F_3 \rightarrow {}^5P_3$ amplitude in this problem is assessed.

PACS number(s): 13.75.Cs, 11.80.Jy, 24.70.+s, 25.10.+s

I. INTRODUCTION

Recently, the $pp \rightarrow p\pi^+ n$ reaction with polarized beam has been studied in the range $p_{\rm beam}^{\rm lab}$=1.18–1.98 GeV/c at the Argonne zero-gradient synchrotron (ZGS) by Wicklund *et al.* [1] (hereafter refered as WI). The aim of this experiment was to shed some light on the controversial issue of the *dibaryon resonances* whose existence was claimed from the structure in proton-proton scattering at intermediate energies. The candidates have been considered as having strong inelastic couplings to the πNN channel, two most eminent of which are assigned to be associated with the $NN\ ^1D_2$ and $^3F_3$ partial waves. Spin-correlation measurements, aimed to investigate this dibaryon problem, were done more recently at LAMPF by Shypit *et al.* [2] at lower energies.

Among the impressive number of *observables* extracted in Ref. [1], some are easily accessible from direct theoretical calculations based on three-body models, namely the data concerning the quasi-two-body reaction $pp \rightarrow \Delta^{++}n$. Indeed, as far as the coupled πNN-NN theory involves the dominant πN-P_{33} (or Δ) input, it is possible to extract the $NN \rightarrow N\Delta$ amplitudes at different values of the Δ mass (viz. the invariant mass of the πN pair in the P_{33} state) in the range allowed by a given incident channel energy, and then to calculate the observables for that reaction. Note, however, that the comparison with the ZGS experimental data is not straightforward as we will explain later.

The coupled πNN-NN model is a unitary model describing in a unified manner the following processes:

$$\begin{Bmatrix} NN \\ \pi d \end{Bmatrix} \rightarrow \begin{Bmatrix} NN \\ \pi d \\ \pi NN. \end{Bmatrix}$$

Extensive calculations based on this model have led to a rather satisfactory overall description of the two-body final-states processes at intermediate energies [3,4]. However, one major deficiency appears in the $NN \rightarrow NN$ channel: the inelasticity parameter is underestimated for $T_N^{\rm lab} \geq 700$ MeV, especially in the $^3F_3$ partial wave, and our attempts at improving this situation by introducing the heavy meson exchange contributions have been unsuccessful [3]. This problem seems to be directly related to the chosen Δ model: there are some recent indications that the $^3F_3$ inelasticity is increased when a two-potential model is used in the P_{33} (in combination with the backward propagating pion contribution), but the effect is still insufficient [4].

The $NN \rightarrow N\Delta$ process is certainly an appropriate reaction for investigation of the Δ model, and the recent ZGS data should provide new informations quite useful for this objective. This is the main aim of the present work. The data we have retained to compare with our model prediction are the following: (i) The differential cross section $d\sigma/d\cos\theta_\Delta$, where θ_Δ denotes the center-of-mass (c.m.) production angle of the Δ, (ii) the differential cross section $d\sigma/dM_{p\pi^+}$, i.e., the $M_{p\pi^+}$ (or the Δ) mass spectrum, for two slices in $\cos\theta_\Delta$, (iii) the production asymmetry parameter $A_y(\cos\theta_\Delta)$, (iv) the s-channel density matrix elements (DME) ρ_{11}, ρ_{33}, ρ_{31}, and ρ_{3-1} as functions of $\cos\theta_\Delta$, (v) the s-channel spin correlations $P_y\rho_{11}$, $P_y\rho_{33}$, $P_y\rho_{31}$, $P_y\rho_{3-1}$, $P_x\rho_{31}$, $P_x\rho_{3-1}$, $P_z\rho_{31}$ and $P_z\rho_{3-1}$ as functions of $\cos\theta_\Delta$ (note that, for example, $P_y\rho_{11}$ is not a product of P_y and ρ_{11}).

These quantities have been evaluated at three different values of the incident kinetic energy: $T_N^{\rm lab} = 0.57$, 0.81, and 1.01 GeV, corresponding respectively to the values 1.18, 1.47, and 1.71 GeV/c of the incident momentum chosen in the experiment.

 ©1993 The American Physical Society

Our results will also be compared with the calculations of Auger *et al.* [5]. These authors have investigated the short-range mechanisms in the $NN \to N\Delta$ reaction by adding in a phenomenological way the ρ-meson exchange contribution to the original iterated pion-exchange model of Kloet and Silbar [6]. They have come to the conclusion that the $NN \to N\Delta$ reaction in the 1 GeV region is less peripheral than usually believed to be.

The present article is organized as follows. Section II is devoted to the theoretical aspects: we give a brief description of the three-body equations for the $NN \to N\Delta$ reaction and of the two-body input used in the P_{11} and P_{33} channels, and we explain how the various observables may be calculated. In Sec. III, we present our results obtained with different Δ models. The effect of the ρ exchange is studied in Sec. IV. In Sec. V, we analyze our results in terms of $NN \to N\Delta$ amplitudes, and our conclusion is drawn in Section VI.

II. THEORETICAL ASPECTS

A. Equations for the $NN \to N\Delta$ reaction

Our starting point is the Avishai-Mizutani unitary model for the coupled πNN-NN systems [7], which we have extensively used to investigate the $\pi d \to \pi d$, $\pi d \leftrightarrow NN$, and $NN \to NN$ reactions at intermediate energy [3]. The basic inputs of this model are the NN and πN interactions, which are assumed to be separable. The two-body partial waves needed to describe correctly the above processes are the πN P_{33} and P_{11} channels, the *small* S and P πN partial waves (i.e., S_{11}, S_{31}, P_{13}, and P_{31}), and of course the NN $^3S_1$-$^3D_1$ (d) channel. The P_{11} channel, where π absorption takes place, is described according to the decomposition of the total t matrix into pole and nonpole parts [8].

As we are interested in the $NN \to N\Delta$ reaction, we consider a *simplified* version of this model where only the πN P_{33} and P_{11} channels are retained, which clearly should dominate this process. So, the equations read in operator form

$$X_{\alpha N} = Z_{\alpha N} + Z_{\alpha N} R_N X_{NN} + \sum_\beta Z_{\alpha\beta} R_\beta X_{\beta N}, \qquad \alpha, \beta \in \{N, \Delta, \Delta'\}. \tag{1}$$

Here, the indices Δ, Δ', and N refer to $N(\pi N)$ three-body channels with the (πN) pair being in the P_{33}, P_{11}(nonpole) and P_{11}(pole) partial waves, respectively. The X are the three-body amplitudes, Z the Born terms (or driving terms), and R the two-body propagators in three-body Hilbert space.

The above equation constitutes a set of coupled equations, leading to the $X_{\Delta N}$ amplitude, which, when evaluated at the *appropriate* Δ on-shell momentum, corresponds to the physical amplitude for $NN \to N\Delta$. In practice, after angular momentum decomposition, we solve a set of coupled one-dimensional integral equations for rotational invariant partial wave amplitudes. We so obtain the physical partial amplitudes:

$$T^J_{l_f \Sigma_f, l_i \Sigma_i}(k_f, k_i; s), \tag{2}$$

where l_i is the relative orbital momentum and Σ_i the channel spin in the NN initial channel, l_f and Σ_f are the corresponding quantities in the $N\Delta$ final channel, and J is the total angular momentum of the system ($\mathbf{J} = \mathbf{l}_i + \mathbf{\Sigma}_i = \mathbf{l}_f + \mathbf{\Sigma}_f$).

In the relativistic approach, $s = 2mT_N^{\rm lab} + 4m^2$ is the c.m. total energy squared (m is the nucleon mass), and $k_i = \sqrt{s/4 - m^2}$ is the on-shell initial momentum. In the final channel, we define the on-shell momentum k_f in terms of the invariant mass squared σ_Δ of the πN pair:

$$k_f = \left[\frac{(s - \sigma_\Delta + m^2)^2}{4s} - m^2\right]^{1/2}. \tag{3}$$

In what follows, we call $\sqrt{\sigma_\Delta}$ as the "Δ mass," which corresponds to the invariant mass $M_{p\pi^+}$ used in WI. In practice, we must vary the Δ mass value within the Δ^{++} bands considered in the ZGS experiment at each incident energy (note that the upper kinematical limit is $\sqrt{\sigma_\Delta} = \sqrt{s} - m$).

B. The P_{11} and P_{33} input

In the P_{11} channel, we use the same parametrization as in Ref. [3] (this paper is hereafter refered to as LY87), namely the total t matrix is written as $t = t_P + t_{\rm NP}$, where t_P is the direct nucleon pole part and $t_{\rm NP}$ the remaining background (or nonpole part). All the details can be found in Ref. [8]. The important fact is that the corresponding three-body channels are treated as different channels, so that the Pauli principle can be applied only to the intermediate NN states coming from the pole part (see Refs. [3,4,9] for the discussions concerning this point).

In the P_{33} channel, we will consider two types of parametrizations. The first one is the usual Δ-isobar model, where the potential is written as one-term separable:

$$V = |v_R\rangle \lambda_R \langle v_R|, \quad \lambda_R = [s - \widetilde{M}_\Delta^2]^{-1}. \tag{4}$$

Here, $\widetilde{M}_\Delta$ is the bare-Δ mass, and s is the πN total energy squared. A monopole form factor is assumed,

$$\langle p|v_R\rangle = g_R(p) = p\,(p^2 + \Lambda_R^2)^{-1}. \tag{5}$$

The second type is a two-potential model where V is written as the sum of two terms,

$$V = v_B + v_R. \tag{6}$$

The resonant interaction v_R has the same expression as in Eq. (4), and the background interaction v_B, which simulates the crossed two-pion process (and possible σ and ρ exchanges), is treated as a purely phenomenological separable potential:

$$v_B = |g_B\rangle \lambda_B \langle g_B| \tag{7}$$

with a monopole form factor:

$$g_B(p) = S_B\, p\,(p^2+\Lambda_B^2)^{-1}. \tag{8}$$

For the resonant part, two types of form factors are considered, namely a dipole form proposed by Tanabe and Ohta (model A in Ref. [10]):

$$\langle p|v_R\rangle = g_R(p) = p\,(p^2+\Lambda_R^2)^{-2}, \tag{9}$$

or a Saxon-Woods form that we have proposed in Ref. [4]:

$$g_R(p) = S_R\, p\left[1+\exp\left(\frac{p^2-p_0^2}{\beta_R^2}\right)\right]^{-1}. \tag{10}$$

In each case, the strength and cut-off parameters are fitted to the experimental phase shifts. Note that the cut-off parameter Λ_R was chosen by Tanabe-Ohta to be 1000 MeV/c. This value corresponds to $\Lambda_R/\sqrt{2} \sim 700$ MeV/c for a monopole form factor, in line with the values used in the model of Lee [11] or in the cloudy bag model [12].

We now briefly recall the reason why the two-potential models should be prefered to the Δ-isobar model (all details can be found in Ref. [4]). In the Δ-isobar model which was used in LY87, the obtained cutoff value is $\Lambda_R \sim 300$ MeV/c. In the πNN equations this gives a too strong cutoff, leading to an underestimation of the effect of pion production. For this reason, *off-shell modifications* where introduced in the LY87 calculations implementing an appropriate off-shell behavior in the P_{33} channel, in order to be consistent with the $\pi d \leftrightarrow NN$ cross section near the Δ resonance energy. A more satisfactory approach to this problem based on a two-potential model for the P_{33} (and P_{11}) was proposed by Tanabe and Ohta [10]. Extending the work of these authors, we have recently shown how it is possible to obtain a coherent description of the πd elastic, $\pi d \leftrightarrow NN$ and $NN \rightarrow NN$ reactions by using in the original LY87 model a two-potential P_{33} in combination with the backward propagating pion contribution, without employing the off-shell modifications (see the results obtained with the LYTO model in Ref. [4]).

C. $NN \rightarrow N\Delta$ observables

Considering the available ZGS data, we adopt the s-channel helicity formalism to express the observables. Following WI, we denote as M, λ_b, λ_t, and λ_n the helicities for the Δ-isobar, beam, target, and recoil (spectator) nucleon, respectively. The partial-wave helicity amplitudes for the T matrix can be expanded in terms of the partial waves in the (LSJ) representation defined in Eq. (2):

$$T^J_{\lambda_n M,\lambda_b\lambda_t} = \sum_{l_f\Sigma_f l_i\Sigma_i} \langle Jl_f\Sigma_f|J\lambda_n M\rangle(-)^{l_f} \times T^J_{l_f\Sigma_f,l_i\Sigma_i}\langle Jl_i\Sigma_i|J\lambda_b\lambda_t\rangle. \tag{11}$$

The coefficients of the unitary transformation connecting the two representations are defined according to the Simonius convention [13],

$$\begin{aligned}\langle Jl_i\Sigma_i|J\lambda_b\lambda_t\rangle &= (-)^{\Sigma_i-\frac{1}{2}+\lambda_b}\langle \tfrac{1}{2}\lambda_b\tfrac{1}{2}-\lambda_t|\Sigma_i\lambda\rangle \\ &\quad\times\langle \Sigma_i-\lambda J\lambda|l_i 0\rangle, \\ \langle Jl_f\Sigma_f|J\lambda_n M\rangle &= (-)^{\Sigma_f-\frac{3}{2}+\lambda_n}\langle \tfrac{1}{2}\lambda_n\tfrac{3}{2}-M|\Sigma_f\mu\rangle \\ &\quad\times\langle \Sigma_f-\mu J\mu|l_f 0\rangle,\end{aligned} \tag{12}$$

where $\lambda = \lambda_b - \lambda_t$ and $\mu = \lambda_n - M$.

The transition matrix in the helicity frame is given by

$$\langle \lambda_n M|F(\theta_\Delta)|\lambda_b\lambda_t\rangle = \sum_J \frac{2J+1}{4\pi} T^J_{\lambda_n M,\lambda_b\lambda_t} d^J_{\lambda\mu}(\theta_\Delta), \tag{13}$$

where d is the usual reduced rotation matrix, and θ_Δ is the c.m. production angle of the Δ.

The phase factor $(-)^{l_f}$ in expression (11) is introduced to make coherent the definition of the final-state momentum in the two bases: in the three-body formalism, $\mathbf{k}_f$ is the momentum of the recoil particle relative to the Δ, while here the definition of θ_Δ implies that $\mathbf{k}_f$ is the momentum of the outgoing Δ, in the total c.m. system in both cases. We note that in the above expressions, we have fixed the $p\pi^+$ pair to be in the Δ state (with spin parity $J^P = \frac{3}{2}^+$), while in WI the nonresonant $J^P = \frac{1}{2}^\pm$ isobars are considered in addition to the Δ.

The parity conservation in production gives the following constraint:

$$\langle -\lambda_n - M\,|F(\theta_\Delta)|\,-\lambda_b-\lambda_t\,\rangle = (-)^{\lambda_b+\lambda_t+\lambda_n+M+1} \times\langle\,\lambda_n M\,|F(\theta_\Delta)|\,\lambda_b\lambda_t\,\rangle, \tag{14}$$

and the Pauli principle imposes the symmetry:

$$\langle \lambda_n M|F(\theta_\Delta)|\lambda_b\lambda_t\rangle = (-)^{\lambda_b+\lambda_t+\lambda_n+M} \times\langle \lambda_n M|F(\pi-\theta_\Delta)|\lambda_t\lambda_b\rangle. \tag{15}$$

We now define the *unnormalized* production density matrix:

$$\rho_{MM'} = \sum_{\lambda_b\lambda_t\lambda_n} \langle \lambda_n M|F|\lambda_b\lambda_t\rangle\langle\lambda_b\lambda_t|F^\dagger|\lambda_n M'\rangle. \tag{16}$$

This is a 4×4 Hermitian matrix with the following symmetry properties:

$$\rho_{MM'} = \rho^*_{M'M}, \quad \rho_{-M-M'} = (-)^{M-M'}\rho_{MM'}. \tag{17}$$

The explicit form of this matrix is the following (we use as indices $2M$ and $2M'$):

$$\rho(3/2) = \begin{pmatrix} \rho_{33} & \rho_{31} & \rho_{3-1} & \rho_{3-3} \\ \rho^*_{31} & \rho_{11} & \rho_{1-1} & \rho^*_{3-1} \\ \rho^*_{3-1} & -\rho_{1-1} & \rho_{11} & -\rho^*_{31} \\ -\rho_{3-3} & \rho_{3-1} & -\rho_{31} & \rho_{33} \end{pmatrix}, \tag{18}$$

where the diagonal elements are real and the anti-diagonal elements are purely imaginary.

Taking the trace of this matrix, $\mathrm{Tr}\rho = 2(\rho_{11}+\rho_{33})$, and multiplying by the usual kinematical and spin-isospin fac-

tors, leads to the differential cross section. In the case of a polarized beam, the spin correlations denoted as $P_i\,\rho_{MM'}$, with $i = x$, y or z, are given by

$$P_i\,\rho_{MM'} = \sum_{\lambda_b\lambda_b'\lambda_t\lambda_n} \langle\lambda_n M|F|\lambda_b\lambda_t\rangle\sigma^{(i)}_{\lambda_b\lambda_b'} \times\langle\lambda_b'\lambda_t|F^\dagger|\lambda_n M'\rangle/\mathrm{Tr}\rho_{MM'}, \quad (19)$$

where $\sigma^{(i)}$ is the Pauli matrix of the polarized proton beam. The left-right asymmetry A_y is

$$A_y = 2P_y\rho_{33} + 2P_y\rho_{11}. \quad (20)$$

The above expressions allow one to calculate the differential cross section, the spin correlations and the asymmetry, as functions of the production angle θ_Δ, at a *given mass* of the Δ. However, the data from the ZGS experiment are the cross sections, asymmetries and spin correlations *integrated* over the Δ^{++} bands. In order to compare our results with these data, we thus define *integrated* quantities where the dispersion in mass of the Δ is taken into account.

The integrated cross section is written as

$$\frac{d\sigma^I}{d\cos\theta_\Delta} = \int_{\sigma_{\min}}^{\sigma_{\max}} \frac{d\sigma}{d\cos\theta_\Delta}\, w(\sigma_\Delta)\, d\sigma_\Delta, \quad (21)$$

where $\sigma_{\min}$ and $\sigma_{\max}$ are the limits of the experimental Δ^{++} band. The weight function $w(\sigma_\Delta)$ is the mass distribution of the Δ. We use the same prescription as Côté *et al.* [14]:

$$w(\sigma_\Delta) = \frac{|f(\sigma_\Delta)|^2}{\int_{(m+m_\pi)^2}^{\infty} |f(\sigma_\Delta)|^2 d\sigma_\Delta}. \quad (22)$$

The f function is the P_{33} $\pi N \to \pi N$ partial wave amplitude, parametrized according to Nagels *et al.* [15],

$$f(u) = \frac{1}{q(u)} \frac{M_\Delta\Gamma(u)}{M_\Delta^2 - u - iM_\Delta\Gamma(u)} \quad (23)$$

with

$$M_\Delta\Gamma(u) = \frac{q^3}{\sqrt{u}} \frac{g^2_{\pi N\Delta}}{4\pi} \frac{B(u = M_\Delta^2)}{B(u)},$$

$$B(u) = 1 + R^2 q^2(u),$$

$$q^2(u) = \frac{1}{4}u\left[1 - \frac{2}{u}(m^2 + m_\pi^2) + \frac{1}{u^2}(m^2 - m_\pi^2)^2\right].$$

We use the same parameters as in Ref. [14], namely R =1 fm, m = 938.26 MeV, m_π = 134.98 MeV, M_Δ = 1232 MeV, and the $\pi N\Delta$ coupling constant is taken from the quark model: $g_{\pi N\Delta} = b\sqrt{18/25}\, g_{\pi NN}$, where the symmetry breaking factor is b = 1.21, and the πNN coupling has the usual value $g^2_{\pi NN}/4\pi = 14.43$.

The integrated asymmetry and spin correlations are defined in the same way.

We have also calculated the $M_{p\pi+}$ mass spectrum by integrating the cross section over the angular range

$$\frac{d\sigma}{dM} = 2\sqrt{\sigma_\Delta}\, w(\sigma_\Delta) \int_a^b \frac{d\sigma}{d\cos\theta_\Delta} d\cos\theta_\Delta, \quad (24)$$

where $M = \sqrt{\sigma_\Delta}$ stands for the Δ mass, and $w(\sigma_\Delta)$ is the mass distribution defined in Eq. (22). The a and b limits are those chosen in the ZGS experiment: two slices in $\cos\theta_\Delta$ have been considered, namely $\cos\theta_\Delta > 0.5$ and $-0.5 < \cos\theta_\Delta < 0.5$.

III. RESULTS

In this section, we present our results for the $NN \to N\Delta$ observables calculated at $T_N^{\rm lab}$ = 0.57, 0.81, and 1.01 GeV with three different models. All models have the P_{11} $(P + NP)$ used in our LY87 calculations and the P_{33} channel. They will be hereafter refered to according to the chosen Δ model: ISO stands for the one-term Δ-isobar model, and TOA and SAX refer to the two-potential models with a dipole (model A from Tanabe-Ohta) or Saxon form factor, respectively (see Sec. II B).

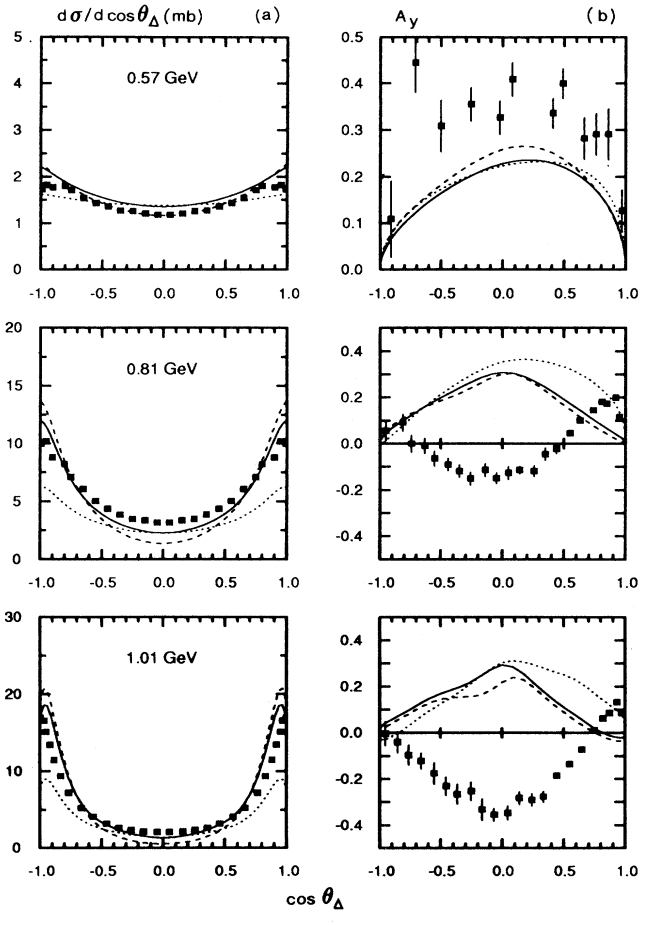

FIG. 1. (a) Integrated differential cross section and (b) production asymmetry A_y for the $NN \to N\Delta$ reaction, calculated at $T_N^{\rm lab}$=0.57, 0.81, and 1.01 GeV with different models. Curves are TOA (solid line), SAX (dashed line), and ISO (dotted line). Data are from Ref. [1].

Note that these models correspond to the *simplified* versions of the models used in our recent paper on the πNN system [4]: ISO corresponds to LY87, and TOA and SAX to LYTO with model A or Saxon parametrizations of the P_{33} , respectively. This means that, apart from the fact that only the P_{11} and P_{33} are retained, other characteristics are the same. In particular, the *backward propagating pion* contribution is taken into account in TOA and SAX, but not in ISO where the *off-shell modifications* are introduced (see Sec. II B).

The integrated differential cross sections are obtained as described in Sec. II C, Eq. (21). The integration is done numerically through Simpson's quadrature of order 3, the σ_Δ values being the lower limit $\sigma_{\min}$, the upper limit $\sigma_{\max}$, and the middle point $(\sigma_{\min}+\sigma_{\max})/2$ of the experimental Δ^{++} band. We use the limits specified in the ZGS experiments, namely $\sqrt{\sigma_{\min}}$ = 1160 MeV, $\sqrt{\sigma_{\max}}$ = 1200 MeV at $T_N^{\rm lab}$ = 0.57 GeV, and $\sqrt{\sigma_{\min}}$ = 1180 MeV, $\sqrt{\sigma_{\max}}$ = 1280 MeV at $T_N^{\rm lab}$ = 0.81 and 1.01 GeV. The results are given in Fig. 1(a) for the three models. Clearly, the ISO model (dotted curve), underestimates the forward (backward) angle cross section at 0.81 and 1.01 GeV by roughly a factor of 2. To a less extent, a similar situation was observed with this model in the $\pi d - NN$ cross section above the Δ resonance [3, 4]. As expected, the underestimation of the effects of pion production which characterizes this model is more apparent in the $NN \rightarrow N\Delta$ reaction. In comparison, the two-potential P_{33} models (combined with the backward pion) give a much better description at all energies. For this reason, we will essentially discuss the TOA and SAX models in what follows. Comparing with the ZGS experimental data, the TOA model (full line) does better than SAX (dashed line), except at 0.57 MeV in the region of the minimum. We note that a clear structure at very forward (backward) angles develops in the theoretical curves as energy increases, although this structure is less evident in the data.

The integrated asymmetries are given in Fig. 1(b). The three models lead to similar results at each of the three considered energies. The results at 0.57 GeV are consistent with the data given the relatively large error bars.

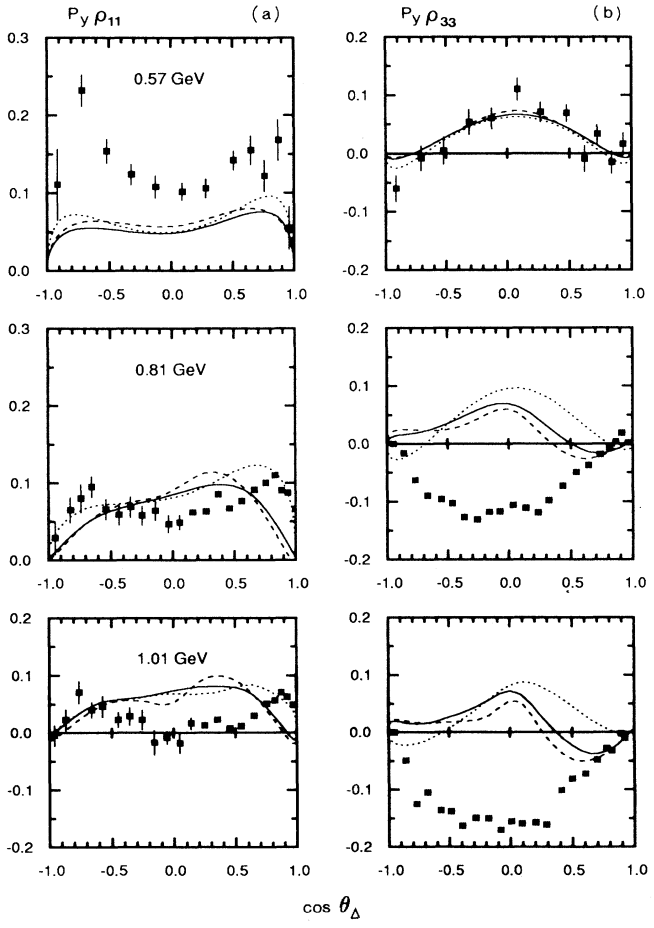

FIG. 2. Integrated spin correlations (a) $P_y\rho_{11}$ and (b) $P_y\rho_{33}$ for the $NN \rightarrow N\Delta$ reaction at $T_N^{\rm lab}$=0.57, 0.81, and 1.01 GeV. Same legend as in Fig. 1.

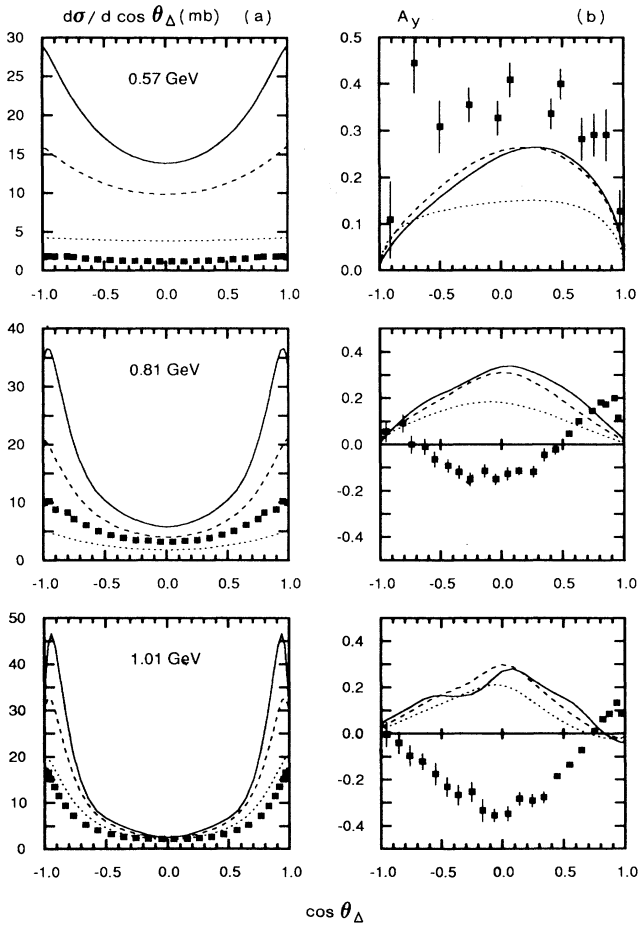

FIG. 3. (a) Differential cross section and (b) production asymmetry A_y for the $NN \rightarrow N\Delta$ reaction, calculated at $T_N^{\rm lab}$ = 0.57, 0.81, and 1.01 GeV with the TOA model at three values of the Δ mass. The values of $\sqrt{\sigma_\Delta}$ (in MeV) are 1160 (solid line), 1180 (dashed line), and 1200 (dotted line) at $T_N^{\rm lab}$=0.57 GeV, and 1180 (solid line), 1230 (dashed line), and 1280 (dotted line) at $T_N^{\rm lab}$=0.81 and 1.01 GeV.

At higher energies, the theoretical calculations stay positive with a broad maximum around $\cos\theta_\Delta = 0$, whereas the data become predominantly negative with a broad minimum around this value.

In Figs. 2(a)–2(b), we show the integrated spin correlations $P_y\rho_{11}$ and $P_y\rho_{33}$ which are the helicity 1/2 and 3/2 contributions to A_y, see Eq. (20). By carefully looking at the experimental data, it appears that $P_y\rho_{33}$ is responsible for the change observed in the A_y structure from positive values at 0.57 GeV to negative values above this energy. Clearly, our present models do inadequately in this helicity 3/2 part: this quantity remains essentially positive as the energy increases, contrary to the data.

To show the dependance of the observables upon the Δ mass, we give in Figs. 3(a)–3(b) the differential cross sections and asymmetries calculated with the TOA model at the three values of σ_Δ defined above for each Δ^{++} band. The cross section is observed to depend strongly upon σ_Δ, so that it only makes sense to compare the integrated value [solid line curves in Fig. 1(a)] with the experimental data. The asymmetry is much less sensitive to σ_Δ, and we see that the results at the middle point of the interval [dashed line in Fig. 3(b)] are almost identical to the integrated values [solid line in Fig. 1(b)].

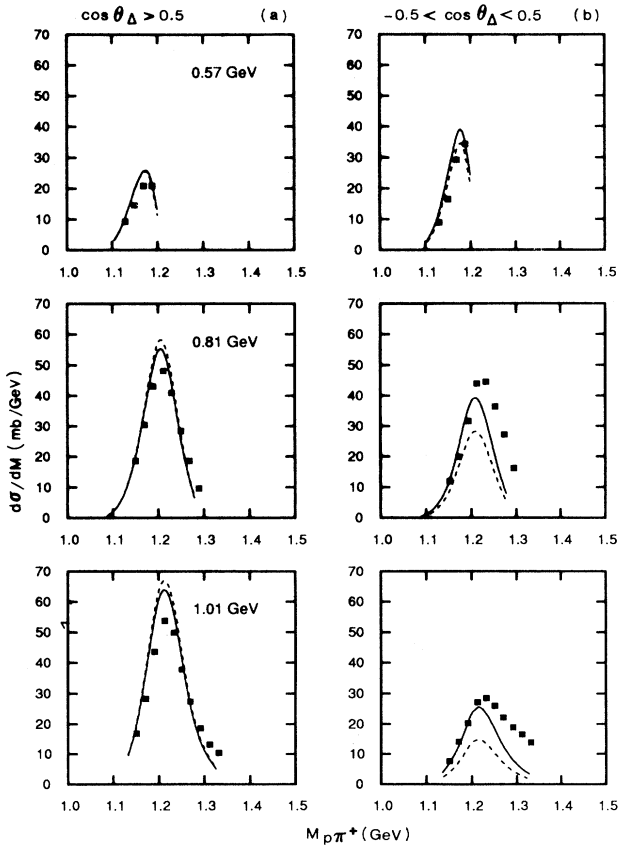

FIG. 4. The $M_{p\pi+}$ mass spectrum calculated at $T_N^{\rm lab}$=0.57, 0.81, and 1.01 GeV with the TOA (solid line) and SAX (dashed line) models, for (a) $\cos\theta_\Delta > 0.5$ and (b) $-0.5 < \cos\theta_\Delta < 0.5$.

The $M_{p\pi+}$ mass spectrum is calculated according to Eq. (24). The differential cross sections are evaluated at various σ_Δ values in the allowed kinematical domain at a given incident energy, and then integrated numerically over $\cos\theta_\Delta$. We show in Figs. 4(a)–4(b) the TOA and SAX results at 0.57, 0.81, and 1.01 GeV, for the two experimental slices in $\cos\theta_\Delta$. For the first slice ($\cos\theta_\Delta > 0.5$), the two models give a correct description of the strong Δ^{++} peak observed experimentally at all energies (only the low side is seen at 0.57 GeV): the width is well reproduced, but the magnitude of the peak is overestimated, this defect increasing with energy. For the second slice ($-0.5 < \cos\theta_\Delta < 0.5$), the two models are in good agreement with the data only at 0.57 GeV. At higher energy, the TOA model does much better than SAX which underestimates the peak by a factor up to ~ 2 at 1.01 GeV. However, only the low side of the Δ^{++} is well reproduced, the magnitude and the width of the peak being underestimated.

Finally, we give in Fig. 5 the integrated DME's ρ_{11}, ρ_{33}, and $\rho_{3\pm1}$, and in Fig. 6 the integrated spin correlations $P_{x,y,z}\rho_{3\pm1}$, calculated at 0.81 GeV with the TOA model (this completes the TOA results given above in Figs. 1 and 2). Concerning the DME's, the calculations reproduce the general trend of the ZGS data. However, the structure at very forward (backward) angles observed in the data (except for ρ_{31}) is not reproduced by the model. Note that the differential cross section is even so good, since it is related to the quantity $\rho_{11}+\rho_{33}$, so that the defects observed in these two quantities compensate. The situation for the spin correlations is far from being satisfactory. The tendency of the model is to give pronounced structures, especially for $P_{x,z}\rho_{3\pm1}$, whereas there are no evident structures in the ZGS data, except for $P_z\rho_{3\pm1}$.

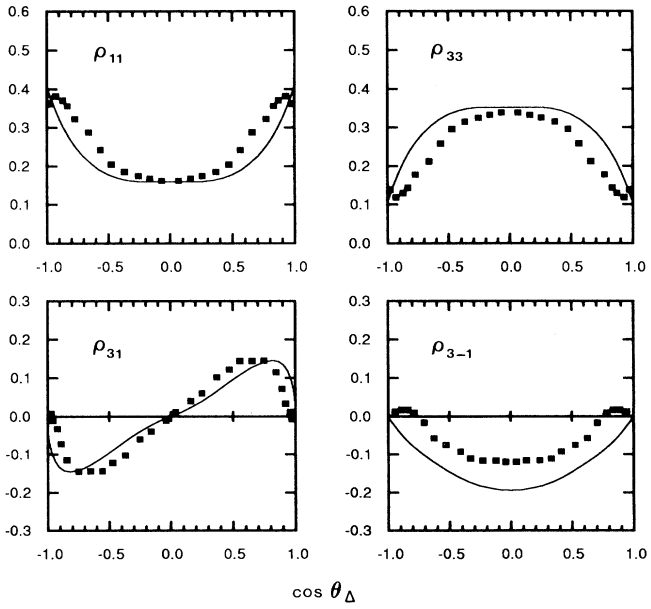

FIG. 5. Integrated DME's for the $NN \rightarrow N\Delta$ reaction calculated at $T_N^{\rm lab}$ =0.81 GeV with the TOA model.

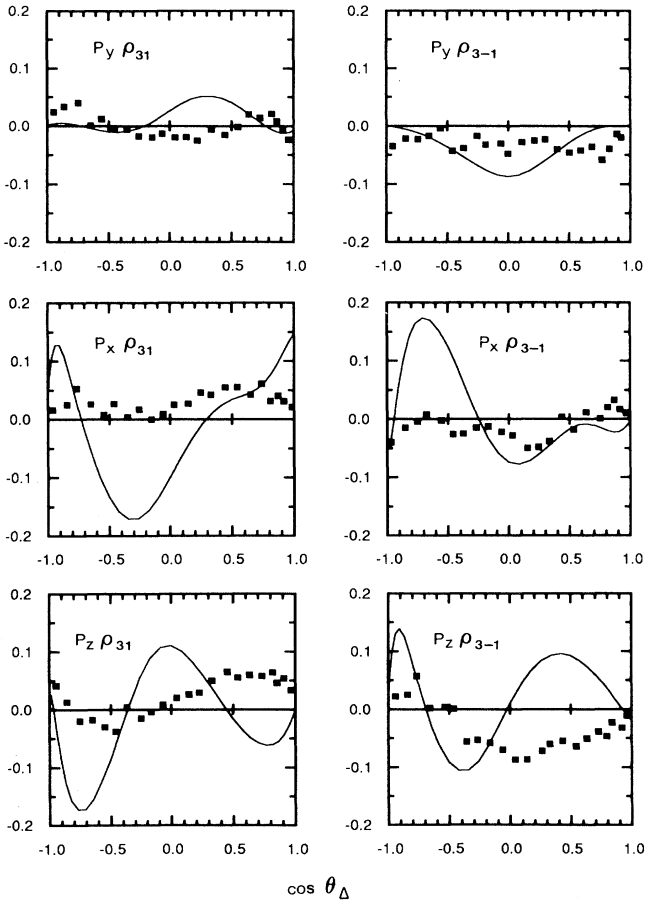

FIG. 6. Integrated spin correlations $P_{x,y,z}\rho_{3\pm1}$ calculated at $T_N^{\rm lab}$=0.81 GeV with the TOA model.

Note that similar conclusions hold when the SAX model is used.

IV. SHORT-RANGE EFFECTS

A. Semiphenomenological approach

The three-body model used above contains the pion exchange iterated to all orders, so that only the long-range part of the interaction is taken into account. It is by now well established that, in order to obtain a correct description of the NN elastic phase parameters within this model, it is necessary to introduce the short-range contribution arising from the exchange of heavy mesons such as ρ, ω, and σ (see Refs. [3, 16]).

Given this situation, Auger *et al.* [5] have recently investigated the short-range effects on the $NN \to N\Delta$ observables. Here we outline the main steps of their semiphenomelogical approach.

(1) The starting point is the three-body model of Kloet and Silbar [6](hereafter denoted as KS). This model gives for the $NN \to N\Delta$ observables a similar trend as our results discussed above (see the dashed line curves in Figs. 2–5 of Ref. [5]), in particular the production asymmetry A_y at 0.81 MeV is large and positive, in contradiction with the ZGS data.

(2) Then, the short-range mechanism is introduced by adding to the KS amplitude a static ρ-exchange contribution in a phenomenological way. Namely, the total $NN \to N\Delta$ scattering matrix is written as

$$M(\text{total}) = M_{\rm KS} + e^{i\Phi} M_\rho, \tag{25}$$

where $M_{\rm KS}$ is the KS three-body amplitude, M_ρ is the $NN \to N\Delta$ transition potential by ρ exchange, and Φ is a relative phase. The form of M_ρ is written following Brown and Weise [17], namely [see Eqs. (13) and (14) in Ref. [5]]

$$M_\rho = (\mathbf{S} \times \mathbf{q}) \cdot (\boldsymbol{\sigma} \times \mathbf{q}) F_\rho(q), \tag{26}$$

where $\mathbf{S}$ and $\boldsymbol{\sigma}$ are respectively the spin 3/2 and spin 1/2 operators, $\mathbf{q}$ is the momentum transfer, and $F_\rho(q)$ is the product of the form factors (of monopole type) times the propagator

$$F_\rho(q) = 4\pi \frac{f_{\rho NN} f_{\rho N\Delta}}{m_\rho^2} \left[\frac{\Lambda^2 - m_\rho^2}{\Lambda^2 + \mathbf{q}^2 - \omega^2} \right]^2 \frac{1}{m_\rho^2 + \mathbf{q}^2 - \omega^2}. \tag{27}$$

In this expression, m_ρ is the ρ-meson mass (fixed to 0.77 GeV), Λ is the cutoff parameter, and $f_{\rho NN}$ and $f_{\rho N\Delta}$ are the coupling constants at the vertices.

(3) At each incident energy, a search has been done for the values of the three quantities: Λ, the product $f_{\rho NN} f_{\rho N\Delta}$ and Φ, by fitting two main observables, namely the asymmetry and the differential cross section.

As explained in Ref. [5], different sets of parameters are obtained: the cutoff parameter Λ varies between 1 and 2 GeV, and correspondingly the product $f_{\rho NN} f_{\rho N\Delta}$ goes from 4–5 (soft ρ) to 10–12 (strong ρ), while the relative phase Φ is found to depend strongly on the energy. The fitted asymmetries and differential cross sections are in very good agreement with the ZGS data at 0.8 and 1.0 GeV. The results for the other selected spin observables (ρ_{11}, $\rho_{3\pm1}$, $P_y\rho_{11}$, and $P_y\rho_{33}$, at 0.8 GeV) are considerably improved in comparison with the pure KS result. In particular, $P_y\rho_{11}$ shows up a pronounced minimum around $\cos\theta_\Delta = 0$ and $P_y\rho_{33}$ becomes negative in the whole angular range, so that the asymmetry $A_y = 2P_y\rho_{11} + 2P_y\rho_{33}$ is now well reproduced.

The important outcome of the work of Auger *et al.* is that apparently the ρ exchange plays an important role in the $NN \to N\Delta$ spin observables. This means that this process is not as peripheral as one would normally expect. However, it is our opinion that the conclusion they have reached must be taken with some care for the following reasons.

(i) The calculations have been done for a single Δ mass. At each energy, the value is chosen to be close to the resonance value ($\sqrt{\sigma_\Delta}$ = 1238 MeV at 0.8 GeV, for example). As discussed in Sec. III, this procedure is not correct, especially for the differential cross section, since the model calculation is compared with the integrated experimental observables.

(ii) The fitted relative phase is found to be close to 0^0 at $T_N^{\rm lab}$=1.0 and 1.25 GeV, which means that the ρ-exchange contribution practically takes on its Born approximation value. This is not the case at 0.8 GeV where the value $\Phi \sim -20^0$ is obtained, indicating that the Born approximation is certainly not valid at this energy.

(iii) The situation at 0.57 GeV has not been examined in Ref. [5]. Our feeling is that the ρ-exchange amplitude will bring the same type of effects as at higher energies, so that the asymmetry A_y, which is correctly reproduced with the KS model, will probably go to the undesirable direction.

B. Iteration of the ρ-exchange to all orders

From the above considerations, it seemed to us necessary to investigate the ρ-exchange contribution within a more satisfactory approach where the ρ is iterated to all orders in the three-body equations, as it is the case for the pion. So, we define for example the $Z_{N\Delta}$ Born term as

$$Z_{N\Delta} = Z^{\pi}_{N\Delta} + Z^{\rho}_{N\Delta}, \tag{28}$$

where $Z^{\pi}_{N\Delta}$ is the usual three-body driving term for one-pion exchange, and $Z^{\rho}_{N\Delta}$ is the driving term for the ρ exchange. The $Z_{\Delta N}$ and $Z_{\Delta\Delta}$ Born terms will be defined similarly (and eventually Z_{NN}, but we have observed that the ρ contribution to this term could be neglected in the first approximation). The method to calculate $Z^{\rho}_{N\Delta}$ can be found in Ref. [18].

We now describe which parameters we have used in the practical calculation. For the ρNN vertex, we choose the same description as in Ref. [3]. The coupling constant is defined as

$$g_{\rho NN} = \left(1 + \frac{g^T}{g^V}\right) g^V, \tag{29}$$

where g^V and g^T are the vector and tensor coupling constants, respectively. We take the values $(g^V)^2/4\pi = 0.5$, and $g^T/g^V = 6.6$, which correspond to the strong ρNN coupling. The cutoff form factor is

$$f(p) = \left(\frac{\Lambda^2 - m_\rho^2}{\Lambda^2 + \mathbf{p}^2}\right)^{3/2}, \tag{30}$$

with the cutoff mass Λ=1650 MeV. We recall here that these values have been chosen (together with the parameters of other heavy mesons) in order to reproduce the $NN\ ^1D_2$ phase shift up to $T_N^{\rm lab} \sim 1$ GeV (see Ref. [3] for more details).

For the $\rho N\Delta$ coupling, we take the SU(4) quark coupling modified by a symmetry breaking factor b:

$$g_{\rho N\Delta} = b\sqrt{\frac{72}{25}}\, g_{\rho NN}, \tag{31}$$

with b=1.2 (see Ref. [14]). The cutoff form factor is the same as for the ρNN vertex.

Note that the f coupling constants used in Ref. [5] are related to the g as follows:

$$f^2_{\rho NN} = \frac{g^2_{\rho NN}}{4\pi}\left(\frac{m_\rho}{2m_N}\right)^2,$$
$$f^2_{\rho N\Delta} = \frac{g^2_{\rho N\Delta}}{4\pi}\frac{m_\rho^2}{4m_N m_\Delta}. \tag{32}$$

Using the above values for the g coupling constants, and taking for the masses m_ρ= 776 MeV, m_N= 938.9 MeV and m_Δ=1232 MeV, we obtain $f^2_{\rho NN} = 4.9$, $f^2_{\rho N\Delta} = 15.6$, which gives $f_{\rho NN} f_{\rho N\Delta} = 8.8$ and $f_{\rho N\Delta}/f_{\rho NN} = 1.8$.

We show in Fig. 7 the results for the integrated differential cross section and production asymmetry at 0.57, 0.81, and 1.01 GeV. The basic model is TOA, which is given by dashed lines (already shown in Fig. 1 as solid lines). Adding the ρ-exchange contribution leads to the solid line curves in Fig. 7. Since it is known that the ρ contribution reduces the effect of the pion exchange, our result for the differential cross section is an expected one, and the agreement with the data still remains acceptable [Fig. 7(a)]. Concerning the asymmetry A_y, the descrip-

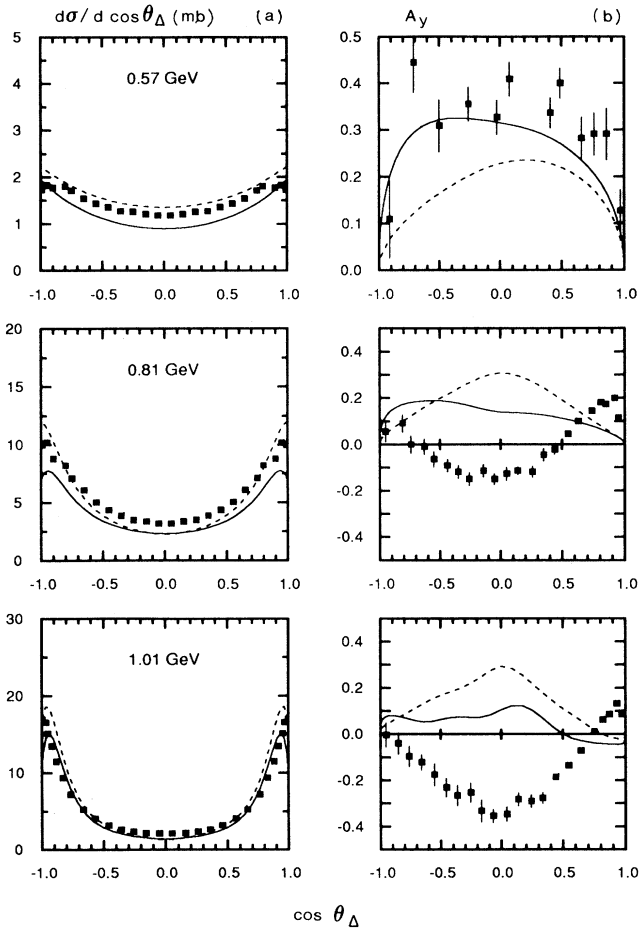

FIG. 7. (a) Integrated differential cross section and (b) production asymmetry A_y for the $NN \to N\Delta$ reaction, calculated at $T_N^{\rm lab}$ = 0.57, 0.81, and 1.01 GeV with the TOA model, with (solid line) or without (dashed line) the ρ-exchange contribution.

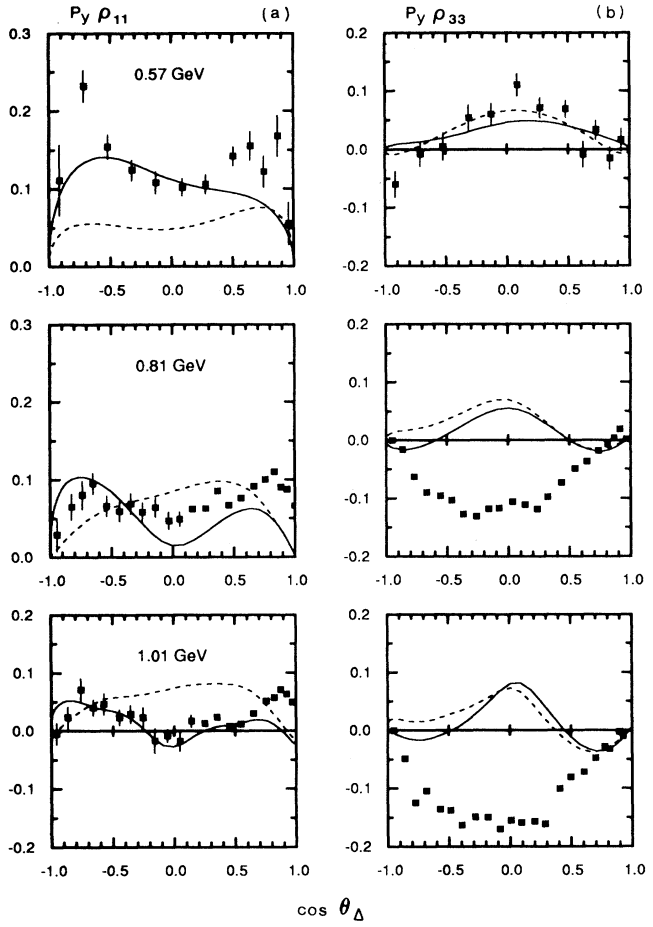

FIG. 8. (a) Integrated spin correlations $P_y\rho_{11}$ and (b) $P_y\rho_{33}$ for the $NN \to N\Delta$ reaction at $T_N^{\rm lab}$=0.57, 0.81, and 1.01 GeV. Same legend as in Fig. 7.

tion of the data at 0.57 GeV is considerably improved when the ρ contribution is taken into account [Fig. 7(b)]. At higher energies, even if this contribution goes in the right direction, the results still remain in disagreement with the ZGS data. To understand the cause of this trouble, it is useful to decompose the asymmetry into $P_y\rho_{11}$ and $P_y\rho_{33}$ as done in the previous section. This is shown in Fig. 8. Then we see a remarkable improvement in $P_y\rho_{11}$ after including the ρ exchange. However, the $P_y\rho_{33}$ spin correlation has changed very little: it does not turn to negative values at 0.81 GeV and above, which is responsible for the undesirable situation for A_y. We note that changing the strength of the ρ essentially affects the magnitude of the differential cross section, but the spin observables are much less sensitive to it. We can thus conclude that the origin of the trouble in reproducing the beam asymmetry A_y is most probably not only due to the short range part of the NN-$N\Delta$ interaction.

V. ANALYSIS IN TERMS OF AMPLITUDES

In this section, we analyze which $NN \to N\Delta$ amplitudes are controlling the observables, in order to better understand the asymmetry problem. All results shown in Secs. III and IV have been obtained as described in Sec. II C, with *all* partial waves included up to $J = 9$ in the expansions leading to the transition matrix in the helicity frame [Eqs. 11) and (13)]. In practice, we have found that retaining all contributions up to $J = 5$ was sufficient to achieve convergence of the observables. The corresponding $NN \to N\Delta$ amplitudes are the following [we use the standard terminology $^{2\Sigma+1}(l)_J$, with l, Σ, J defined in Sec. II A]:

$$
\begin{aligned}
&{}^1S_0 \to {}^5D_0,\\
&{}^3P_0 \to {}^3P_0,\\
&{}^3P_1 \to {}^3P_1\ ,\ {}^5P_1\ ,\ [{}^5F_1],\\
&{}^3P_2 \to {}^3P_2\ ,\ {}^5P_2\ ,\ [{}^3F_2\ ,\ {}^5F_2],\\
&{}^1D_2 \to {}^5S_2\ ,\ {}^3D_2\ ,\ {}^5D_2\ ,\ [{}^5G_2],\\
&{}^3F_2 \to {}^3P_2\ ,\ {}^5P_2\ ,\ {}^3F_2\ ,\ [{}^5F_2],\\
&{}^3F_3 \to {}^5P_3\ ,\ {}^3F_3\ ,\ [{}^5F_3\ ,\ {}^5H_3],\\
&{}^3F_4 \to {}^3F_4\ ,\ {}^5F_4\ ,\ [{}^3H_4\ ,\ {}^5H_4],\\
&{}^1G_4 \to {}^5D_4\ ,\ [{}^3G_4\ ,\ {}^5G_4\ ,\ {}^5I_4],\\
&{}^3H_4 \to {}^3F_4\ ,\ {}^5F_4\ ,\ [{}^3H_4\ ,\ {}^5H_4],\\
&{}^3H_5 \to {}^5F_5\ ,\ [{}^3H_5\ ,\ {}^5H_5\ ,\ {}^5J_5].
\end{aligned}
$$

Now, it is interesting to select among the above 37 amplitudes the dominant ones. We consider the quantity $\sqrt{2J+1}\ |T^J_{NN\to N\Delta}|$, which takes on its maximum value in the ${}^3F_3 \to {}^5P_3$ amplitude for the TOA model at $T_N^{\rm lab}$ = 0.81 GeV. So, we characterize the degree of dominance of each amplitude by the ratio

$$R^J_{NN\to N\Delta} = \sqrt{2J+1}\ |T^J_{NN\to N\Delta}|/\sqrt{7}\ |T_{^3F_3\to {}^5P_3}|. \quad (33)$$

We give in Fig. 9 the bar chart (empty bars) of R^J for the dominant amplitudes, namely those which have $R^J \geq 0.06$. This condition eliminates the amplitudes

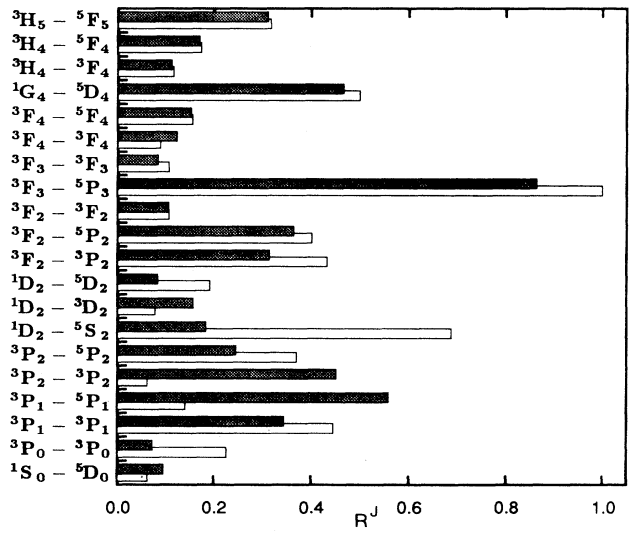

FIG. 9. Bar chart for the dominant quantities $R^J_{NN\to N\Delta}$ [Eq. (33)] at $T_N^{\rm lab}$=0.81 GeV. The TOA model is used, without (empty bars) or with (dashed bars) the ρ contribution.

TABLE I. Dominant $NN \rightarrow N\Delta$ amplitudes at $T_N^{\rm lab} = 0.81$ GeV. The TOA model is used, with or without the ρ-exchange contribution. The numbers 1, 2, etc. ... point out the most dominant amplitudes, in decreasing order of magnitude.

$NN \rightarrow N\Delta$	TOA	TOA+ρ-ex.
$^1S_0 \rightarrow {}^5D_0$	...	...
$^3P_0 \rightarrow {}^3P_0$	...	...
$^3P_1 \rightarrow {}^3P_1$	4	6
$^3P_1 \rightarrow {}^5P_1$	...	2
$^3P_2 \rightarrow {}^3P_2$	...	4
$^3P_2 \rightarrow {}^5P_2$	7	9
$^1D_2 \rightarrow {}^5S_2$	2	10
$^1D_2 \rightarrow {}^3D_2$	...	...
$^1D_2 \rightarrow {}^5D_2$	...	...
$^3F_2 \rightarrow {}^3P_2$	5	7
$^3F_2 \rightarrow {}^5P_2$	6	5
$^3F_2 \rightarrow {}^3F_2$	...	...
$^3F_3 \rightarrow {}^5P_3$	1	1
$^3F_3 \rightarrow {}^3F_3$	...	...
$^3F_4 \rightarrow {}^3F_4$	...	...
$^3F_4 \rightarrow {}^5F_4$	...	...
$^1G_4 \rightarrow {}^5D_4$	3	3
$^3H_4 \rightarrow {}^3F_4$	...	...
$^3H_4 \rightarrow {}^5F_4$	...	...
$^3H_5 \rightarrow {}^5F_5$	8	8

shown in brackets in the above list, leading to the 20 amplitudes listed in the first column of Table I. Among these 20 amplitudes, 8 of them clearly appear as dominant on Fig. 9. They are numbered from 1 to 8 in decreasing order of magnitude in the second column of Table I. This dominance is illustrated in Fig. 10 where we compare the integrated differential cross section and asymmetry parameter calculated at 0.81 GeV with the full set of amplitudes (up to $J = 9$, solid line curves), and with the sets of 20 (dashed line) and 8 (dotted line) dominant amplitudes. We see that the set of 8 amplitudes gives effectively the dominant contribution to the observables. It should be noted that (i) the very peripheral amplitudes $^1G_4 \rightarrow {}^5D_4$ and $^3H_5 \rightarrow {}^5F_5$ must be included in order to obtain the correct magnitude for the cross section, but they have a negligible effect on the polarization parameters, and (ii) the purely central $J = 0$ amplitudes have a negligible contribution to the cross section and a rather small effect on the polarizations.

Similar conclusions hold for the amplitudes where the ρ-exchange contribution is included as described in Sec. IV B. Applying the same criterion as before for selecting the dominant amplitudes, we find the same 20 amplitudes as above (see first column in Table I), only the magnitudes (and eventually the signs) of the real and imaginary parts are changed, depending on the amplitude (this point is examined later). The "global" changes due to the ρ exchange are shown in Fig. 9 where we have plotted the clustered bar chart for the corresponding quantities R^J (dashed bars). Comparing with the values calculated without the ρ contribution (empty bars), we see that the ρ exchange lowers the 8 dominant amplitudes defined above in the second column of Table I, especially $^1D_2 \rightarrow {}^5S_2$, while $^3P_1 \rightarrow {}^5P_1$ and $^3P_2 \rightarrow {}^3P_2$ are strongly enhanced up to rank among the dominant amplitudes. So, we have now the 10 dominant amplitudes numbered from 1 to 10 (in decreasing order of magnitude) in the third column of Table I. We give in Fig. 11 the integrated cross section and asymmetry calculated at 0.81 GeV with the full set of amplitudes (solid line curves), and with the sets of 20 (dashed line), 10 (dash-dotted line), or 8 (dotted line) dominant amplitudes. The effects due to the $^3P_1 \rightarrow {}^5P_1$ and $^3P_2 \rightarrow {}^3P_2$ partial waves appear clearly by comparing the dotted and dash-dotted curves. In particular, we note the change in the structure of A_y (as we will see later, this is due to the $^3P_1 \rightarrow {}^5P_1$ amplitude).

Now that we have selected the dominant amplitudes, we examine to which of them the observables are especially sensitive. To achieve this aim, we compare in de-

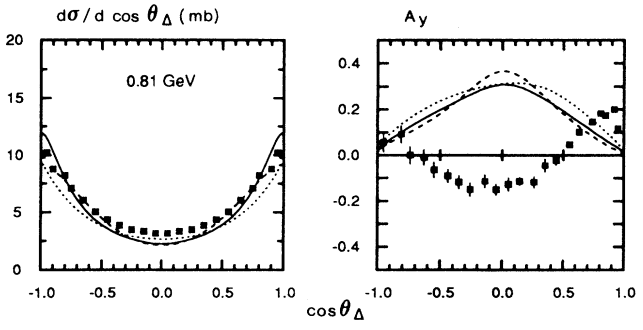

FIG. 10. Integrated differential cross section and production asymmetry A_y for the $NN \rightarrow N\Delta$ reaction, calculated at $T_N^{\rm lab}$=0.81 GeV with the TOA model. The retained amplitudes are full set (solid line), 20 dominant amplitudes from first column in Table I (dashed line), and 8 dominant amplitudes from second column in Table I (dotted line).

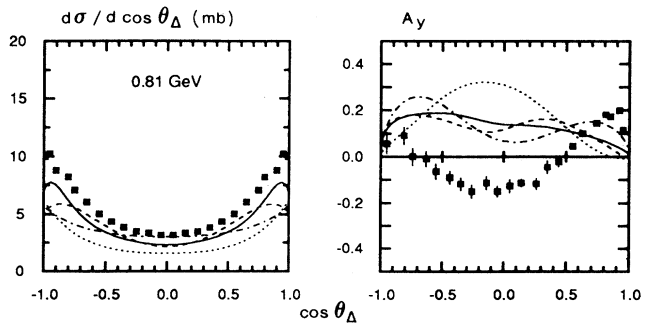

FIG. 11. The same as in Fig. 10, but the ρ contribution is included. The dash-dotted curves correspond to the set of 10 dominant amplitudes from third column of Table I. The legend for the other curves is the same as in Fig. 10.

tail the results obtained *with* and *without* the ρ-exchange contribution. The differences on the observables have been already shown in Sec. IV B, Figs. 7 and 8. We first consider the cross section $d\sigma$ which is controlled by the square moduli of amplitudes. Looking back to Fig. 9, it is clear that the lowering of $d\sigma$ when the ρ exchange is introduced is due to the systematic decrease observed on the 8 dominant amplitudes defined above. In fact, this decrease comes mostly from $^3P_1 \rightarrow {}^3P_1$, $^1D_2 \rightarrow {}^5S_2$, and $^3F_3 \rightarrow {}^5P_3$, and it is only partially compensated by the strong enhancement in $^3P_1 \rightarrow {}^5P_1$ and $^3P_2 \rightarrow {}^3P_2$. Next, we consider the polarization observables, namely the asymmetry A_y and its two components $P_y\rho_{11}$ and $P_y\rho_{33}$. As we have seen in Fig. 8, the ρ contribution improves significantly the description of $P_y\rho_{11}$ at 0.81 GeV, but has little effect on $P_y\rho_{33}$ which remains essentially positive, and the resulting A_y is slightly improved as already shown in Fig. 7. As the polarization observables are sensitive to the relative phases of amplitudes, these differences must be analyzed by comparing the *real* and *imaginary* parts of the dominant amplitudes calculated *with* and *without* the ρ exchange. The corresponding bar chart for the 10 dominant amplitudes defined in Table I (third column) is given in Fig. 12, where we have added the $J = 0$ amplitudes, namely $^1S_0 \rightarrow {}^5D_0$ and $^3P_0 \rightarrow {}^3P_0$. As expected, the ρ-exchange contribution is important in the $J \leq 2$ central partial waves. We note that for $J = 0$, even if the ρ contribution is large in relative value (especially in the $^3P_0 \rightarrow {}^3P_0$ channel), the effect on the observables is small since these amplitudes are far from being dominant. The most spectacular effects due to the ρ contribution appear on the $^3P_1 \rightarrow {}^3P_1$, $^3P_1 \rightarrow {}^5P_1$, $^3P_2 \rightarrow {}^3P_2$, and $^1D_2 \rightarrow {}^5S_2$ amplitudes. We note in particular (i) the strong decrease of the imaginary part of $^3P_1 \rightarrow {}^3P_1$, (ii) the large increase together with the change of sign in both the real and imaginary parts of $^3P_1 \rightarrow {}^5P_1$, and (iii) the large increase of the real and imaginary parts of $^3P_2 \rightarrow {}^3P_2$ together with the change of sign of the real part. By checking the individual effect of these last three amplitudes on the polarization observables, no significant change was observed in $P_y\rho_{33}$, and the $^3P_1 \rightarrow {}^5P_1$ *alone* was found to be responsible for the considerable improvement observed in $P_y\rho_{11}$.

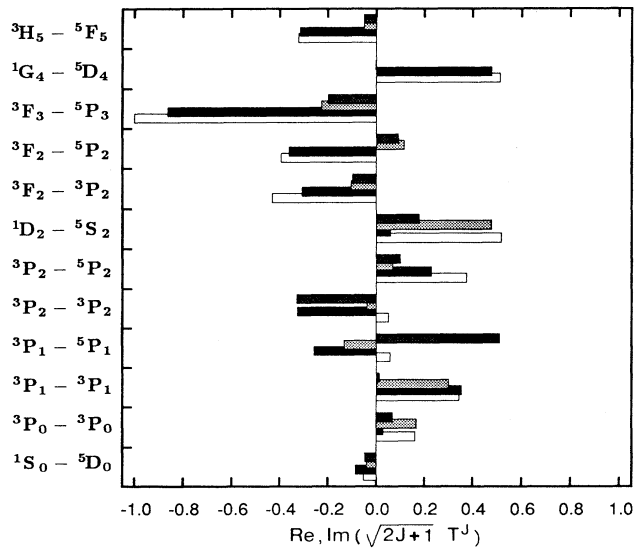

FIG. 12. Bar chart for the real and imaginary parts of the quantities $\sqrt{2J+1}\, T^J_{NN\rightarrow N\Delta}$ at $T_N^{\rm lab}$=0.81 GeV with the TOA model. The legend is real part *without* (empty bars) or *with* (black bars) the ρ contribution, imaginary part *without* (dashed bars) or *with* (dark dashed bars) the ρ contribution. All quantities are normalized to $\sqrt{7}\,\mathrm{Re}(T_{^3F_3 \rightarrow {}^5P_3})$, calculated without the ρ contribution.

We point out that the same type of investigation has been done at 0.57 GeV, leading to similar conclusions. We now summarize what emerges from the above discussion:

(i) The $NN \rightarrow N\Delta$ observables are controlled by a limited number of amplitudes (~ 10), ranging from central up to peripheral J values,

(ii) The peripheral amplitudes are needed to obtain the correct magnitude of the cross section as energy increases, but have little effect on the polarizations,

(iii) The short-range contribution simulated by the ρ exchange affects significantly the central amplitudes, but the corresponding effects on the polarization parameters are moderate. In particular, the $P_y\rho_{33}$ spin correlation is quite insensitive to the various models investigated. The only sensitive quantity is $P_y\rho_{11}$ whose shape appears to be controlled by the $^3P_1 \rightarrow {}^5P_1$ central amplitude alone.

Of course, these conclusions are valid within the framework of our model, and they cannot be taken as definitive, especially regarding point (iii). Certainly, the polarization parameters must be sensitive to other amplitudes besides $^3P_1 \rightarrow {}^5P_1$. In particular, the $^3F_3 \rightarrow {}^5P_3$ amplitude, which is dominant at 0.81 GeV, is expected to play an important role in the construction of the polarization observables at this energy. This can be demonstrated in the following way. At first, we turn off its contribution in the calculation of the observables at 0.81 GeV (the TOA model is used, without the ρ contribution). The results are shown in Fig. 13 (dashed line curves) and compared with the full calculation (solid line). Of course, the differential cross section is lowered, but the most spectacular effect appears on A_y which becomes negative with a large and broad minimum around $\cos\theta_\Delta = 0$, in line with the experimental data. This is due to the combined effects on $P_y\rho_{11}$ and $P_y\rho_{33}$ which are both negative in the whole angular range, as shown in Fig. 13. The problem is that $P_y\rho_{11}$ is now in complete disagreement with the data, while $P_y\rho_{33}$ is reasonably reproduced. Next, we have *arbitrarily* modified the $^3F_3 \rightarrow {}^5P_3$ contribution, in order to get intermediate results between the full line and dashed line curves of Fig. 13. We have found that this was possible by lowering the real part together with increasing the imaginary part of this amplitude. As an example, we show in Fig. 13 the results when the real part is multiplied by 0.5 and the imaginary part by 1.5 (dotted line): $P_y\rho_{11}$ is in line with the data, $P_y\rho_{33}$ starts small positive and has a broad negative minimum which is shifted and too high compared to the data, and A_y is in qualitative agreement with the data. The interesting point is that the shape of $P_y\rho_{33}$ appears to be controlled

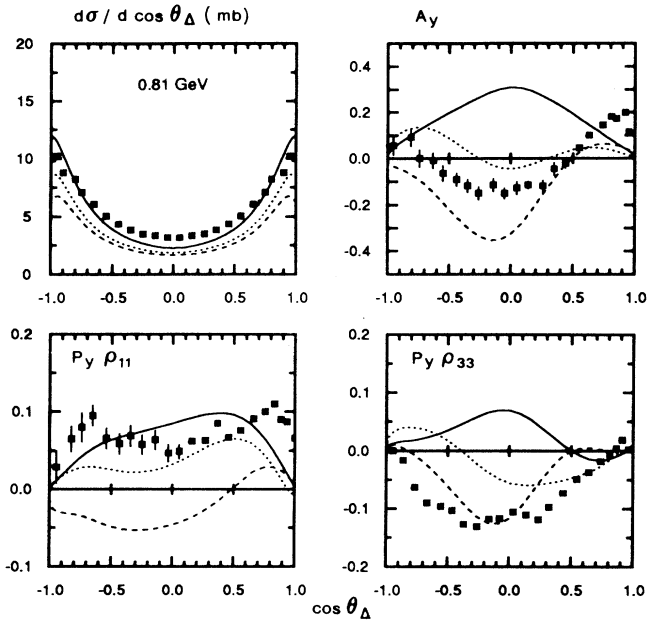

FIG. 13. Integrated differential cross section, production asymmetry A_y, and spin correlations $P_y\rho_{11}$ and $P_y\rho_{33}$ for the $NN \rightarrow N\Delta$ reaction, calculated at $T_N^{\rm lab}$=0.81 GeV with the TOA model, without the ρ contribution. The full set of amplitudes is used (solid line), the $^3F_3 \rightarrow {}^5P_3$ amplitude is omitted (dashed line), the real part of $^3F_3 \rightarrow {}^5P_3$ is arbitrarily multiplied by 0.5 and the imaginary part by 1.5 (dotted line).

by the relative magnitude of the real and imaginary parts of the $^3F_3 \rightarrow {}^5P_3$ amplitude. We point out that *none* of the other dominant amplitudes was found able to induce a negative minimum in $P_y\rho_{33}$ when arbitrarily modifying its real and imaginary parts.

VI. CONCLUSION

In this paper, we have studied the $NN \rightarrow N\Delta$ reaction within the unitary three-body approach which was successfully used in previous works to describe the πNN system. This investigation confirms our findings in Ref. [4] that a two-potential description of the P_{33} πN channel, combined with the backward propagating pion contribution, is better than the usual one-term Δ-isobar model. The global agreement of our results with the available Argonne ZGS data at $T_N^{\rm lab}$ = 0.57, 0.81, and 1.01 GeV is rather satisfactory. Our results for the integrated differential cross sections are in good agreement with the data at the three considered energies. The main problem concerns the integrated asymmetry A_y which is consistent with the data only at 0.57 GeV. At higher energies, the theoretical model is unable to reproduce the broad negative minimum observed in the data around $\cos\theta_\Delta = 0$.

Our attempt to improve this situation by introducing the short-range effects arising from the ρ-exchange contribution can be considered as partially successful. The helicity 1/2 component of A_y, namely $P_y\rho_{11}$, is remarkably improved at the three energies, but the helicity 3/2 part $P_y\rho_{33}$ is quite insensitive to the ρ contribution. The resulting A_y is considerably improved at 0.57 GeV, but the discrepancy with the data still remains at higher energies, even if a slight improvement is observed.

The asymmetry problem at high energy is directly related to the fact that none of the used models (even including the ρ contribution) is able to describe $P_y\rho_{33}$. The difficulty in determining which $NN \rightarrow N\Delta$ amplitudes are responsible for this situation is that the construction of the observables involves both central and peripheral contributions. However, we have identified a limited number of dominant amplitudes, and we have shown that two of them play an important role in the polarization sector, namely the central $^3P_1 \rightarrow {}^5P_1$ and the peripheral $^3F_3 \rightarrow {}^5P_3$. The $^3P_1 \rightarrow {}^5P_1$ amplitude controls the $P_y\rho_{11}$ spin correlation. This effect was observed by introducing the ρ contribution which has a strong influence on this central wave. The $^3F_3 \rightarrow {}^5P_3$ amplitude appears to be responsible for the incorrect description of $P_y\rho_{33}$, and thus of A_y, at 0.81 GeV. This was clearly demonstrated by modifying "by hand" the real and imaginary parts of this amplitude. The problem is that none of the models investigated is able to bring such variations in this amplitude, in particular the ρ contribution has no significant effect on this peripheral wave.

The deficiency of the model to reproduce the change from a broad positive maximum to a broad negative minimum observed in the $P_y\rho_{33}$ experimental data as energy increases is certainly associated with the *spin-triplet problem* already encountered in the NN elastic sector (namely the lack of inelasticity in the $^3F_3$ channel for $T_N^{\rm lab} \geq 700$ MeV). Now, the question arises that maybe some fundamental mechanism is missing in the three-body approach. One possible mechanism is the *direct* $N\Delta$ interaction between the nucleon and the Δ isobar. Recently, Alexandrou and Blankleider [19], and Peña *et al.* [20] have investigated the effects of such an interaction on the observables of the πNN system. Even if the description of the instantaneous $N\Delta$ potential is done differently, the conclusions of the two groups are similar. In general, strong effects are observed on the πNN observables in the intermediate energy range. Nevertheless, the NN $^3F_3$ inelasticity is not improved. In the $NN \rightarrow N\Delta$ sector, the interesting point is that the change in the structure of A_y observed experimentally when energy increases is induced by the $N\Delta$ potential. However, the agreement with the data at $T_N^{\rm lab}$=0.81 GeV remains qualitative (see Fig. 14 in Ref. [20]). Obviously, further investigations are needed to have a better control over this mechanism, in particular to find a procedure for determining the parameters of the $N\Delta$ interaction. In our opinion, this is a promising direction for further studies in the near future.

ACKNOWLEDGMENTS

One of us (T.M.) is grateful to CEN Saclay and IPN Lyon, France, for offering him a few visits in the course of this work. Another (C.F.) is thankful to the Physics Department, VPI & SU for kind hospitality during his visit there. A partial support by the U.S. Department of Energy under Grant No. DE-FG-ER40413 is greatly appreciated.

[1] A. B. Wicklund *et al.*, Phys. Rev. D **35**, 2670 (1987).
[2] R. L. Shypit *et al.*, Phys. Rev. Lett. **60**, 901 (1988); Phys. Rev. C **40**, 2203 (1989).
[3] G. H. Lamot, J. L. Perrot, C. Fayard, and T. Mizutani, Phys. Rev. C **35**, 239 (1987).
[4] C. Fayard, G. H. Lamot, T. Mizutani, and B. Saghai, Phys. Rev. C **46**, 118 (1992).
[5] J. P. Auger, C. Lazard, and R. J. Lombard, Phys. Rev. D **39**, 763 (1989).
[6] W. M. Kloet and R. R. Silbar, Nucl. Phys. A **338**, 281 (1980); **364**, 346 (1981).
[7] Y. Avishai and T. Mizutani, Nucl. Phys. A **326**, 352 (1979); **338**, 377 (1980).
[8] T. Mizutani, C. Fayard, G. H. Lamot, and R. S. Nahabetian, Phys. Rev. C **24**, 2633 (1981).
[9] T. Mizutani, C. Fayard, G. H. Lamot, and B. Saghai, Phys. Rev. C **40**, 2763 (1989).
[10] H. Tanabe and K. Ohta, Nucl. Phys. A **484**, 493 (1988); Phys. Rev. C **36**, 2495 (1987).
[11] T.-S. H. Lee, Phys. Rev. C **29**, 195 (1984).
[12] S. Théberge, A. W. Thomas, and G. A. Miller, Phys. Rev. D **22**, 2838 (1980).
[13] M. Simonius, in *Polarization Nuclear Physics*, edited by D. Fick, Lecture Notes in Physics Vol. 30 (Springer-Verlag, Berlin, 1974).
[14] J. Côté, M. Lacombe, B. Loiseau, and W. N. Cottingham, Nucl. Phys. A **379**, 349 (1982).
[15] M. M. Nagels *et al.*, Nucl. Phys. B **147**, 189 (1979).
[16] W. M. Kloet and R. R. Silbar, Phys. Rev. Lett. **45**, 970 (1980).
[17] G. E. Brown and W. Weise, Phys. Rep. **22C**, 279 (1975).
[18] A. S. Rinat, E. Hammel, Y. Starkand, and A. W. Thomas, Nucl. Phys. A **329**, 285 (1979).
[19] C. Alexandrou and B. Blankleider, Phys. Rev. C **42**, 517 (1990).
[20] M. T. Peña, H. Garcilazo, U. Oelfke, and P. U. Sauer, Phys. Rev. C **45**, 1487 (1992).